2019

Synthesis of Sea Urchin-Like NiCo2O4 via Charge-Driven Self-Assembly Strategy for High Performance Lithium-Ion Batteries

Bin Wang
Hong Kong Applied Science and Technology Research Institute, Hong Kong, China

Chi-Wing Tsang
Technological and Higher Education Institute of Hong Kong (THEi), ctsang@vtc.edu.hk

Ka Ho Li
Technological and Higher Education Institute of Hong Kong (THEi)

Yuanyuan Tang
Southern University of Science and Technology

Yanping Mao
Shenzhen University

See next page for additional authors

Recommended Citation

Wang, B.,Tsang, C.,Li, K.,Tang, Y.,Mao, Y.,& Lu, X. (2019). Synthesis of Sea Urchin-Like NiCo2O4 via Charge-Driven Self-Assembly Strategy for High Performance Lithium-Ion Batteries. *Nanoscale Research Letters, 14* (6), 1-9. http://dx.doi.org/10.1186/s11671-018-2819-4

Nanoscale Research Letters

NANO EXPRESS Open Access

Synthesis of Sea Urchin-Like $NiCo_2O_4$ via Charge-Driven Self-Assembly Strategy for High-Performance Lithium-Ion Batteries

Bin Wang[2], Chi-Wing Tsang[1], Ka Ho Li[1], Yuanyuan Tang[3], Yanping Mao[4] and Xiao-Ying Lu[1*]

Abstract

In this study, hydrothermal synthesis of sea urchin-like $NiCo_2O_4$ was successfully demonstrated by a versatile charge-driven self-assembly strategy using positively charged poly(diallydimethylammonium chloride) (PDDA) molecules. Physical characterizations implied that sea urchin-like microspheres of ~ 2.5 μm in size were formed by self-assembly of numerous nanoneedles with a typical dimension of ~ 100 nm in diameter. Electrochemical performance study confirmed that sea urchin-like $NiCo_2O_4$ exhibited high reversible capacity of 663 mAh g^{-1} after 100 cycles at current density of 100 mA g^{-1}. Rate capability indicated that average capacities of 1085, 1048, 926, 642, 261, and 86 mAh g^{-1} could be achieved at 100, 200, 500, 1000, 2000, and 3000 mA g^{-1}, respectively. The excellent electrochemical performances were ascribed to the unique micro/nanostructure of sea urchin-like $NiCo_2O_4$, tailored by positively charged PDDA molecules. The proposed strategy has great potentials in the development of binary transition metal oxides with micro/nanostructures for electrochemical energy storage applications.

Keywords: Hydrothermal synthesis, $NiCo_2O_4$, Self-assembly, Lithium-ion batteries

Introduction

Spinel nickel cobaltite ($NiCo_2O_4$) is one of the most important binary transition metal oxides (TMOs) with wide applications in electro-catalytic water splitting, supercapacitors and rechargeable battery materials, etc. [1–7]. Particularly, spinel $NiCo_2O_4$, having a theoretical specific capacity (890 mAh g^{-1}), can be used as promising high-capacity anode materials for electrochemical lithium storage, owing to the higher electrical conductivity and electrochemical activities than monometallic oxides (Co_3O_4 and NiO) [8, 9]. However, lithium storage performance of $NiCo_2O_4$ was highly dependent on the distinct structure and morphology, which showed significant effects on cycling stability and rate capability.

In recent years, various $NiCo_2O_4$ with interesting morphologies, including nanowires [10], nanosheets [11], nanoflakes [12], nanobelts [12], sea urchin-like [13], and flower-like structures [14], have been synthesized by hydrothermal and solvothermal method. Previous studies suggested that micro/nanostructures manifested dual benefits from microscale and nanoscale dimensions for improved electron and ion transport, thereby leading to superior electrochemical performances [15, 16]. Generally, structure design of $NiCo_2O_4$ with micro/nanostructures was directed by choosing appropriate morphology controlling reagents. Zhang et al. employed polyvinylpyrrolidone (PVP) to synthesize $NiCo_2O_4$ for controlling morphology, based on coordination of metal ions with functional groups (e.g., -N and/or C=O) of pyrrolidone [17]. However, limited effective structure directing reagents are feasible for synthesis of binary TMOs with unique morphology. Thus, it is highly desirable to explore versatile reagents for synthesizing $NiCo_2O_4$ with micro/nanostructures. Recently, we reported positively charged reagents, such as diallyldimethylammonium chloride (DDA) and its homopolymer, exhibited potentials in synthesizing Co_3O_4 for lithium-ion batteries (LIBs) [15, 16]. However, we are not aware of any binary TMOs (e.g., $NiCo_2O_4$) with micro/nanostructures synthesized by such

* Correspondence: xylu@vtc.edu.hk
[1]Faculty of Science and Technology, Technological and Higher Education Institute of Hong Kong, Hong Kong, People's Republic of China
Full list of author information is available at the end of the article

charged molecules for electrochemical lithium storage applications.

Herein, we reported charge-driven self-assembly strategy for $NiCo_2O_4$ with sea urchin-like structure, followed by thermal treatment. The positively charged poly(diallydimethylammonium chloride) (PDDA) molecules were considered as a crucial structure directing reagent in hydrothermal synthesis. Sea urchin-like $NiCo_2O_4$ with micro/nanostructures also demonstrated superior lithium storage performance in repeated charge-discharge cycles. Obviously, it is the first work on charge-driven self-assembly synthesis of binary TMOs with assistance of charged organic molecules. This novel strategy is expected to pave a new way of synthesizing binary TMOs with novel micro/nanostructures for energy storage materials.

Methods

Synthesis of Sea Urchin-Like $NiCo_2O_4$

In a typical synthesis, 0.5 g of nickel acetate tetrahydrate (≥ 99%), 1.0 g of cobalt acetate tetrahydrate (≥ 98%), and 3.0 g of urea (99.5%) received from Acros Organics were dissolved in 55 mL deionized water, followed by adding 5 g PDDA solution (20 wt.% in H_2O, Sigma-Aldrich). The mixed solution was carefully transferred into a sealed Teflon-lined stainless steel autoclave and placed in an electric oven maintained at 120 °C for 2 h. The resulting precipitation was collected by vacuum-assisted filtration and washed with deionized water for three times. Finally, the filtered sample was thermal treated in a muffle furnace at 450 °C for 2 h. The as-synthesized black samples were directly used in material characterizations and electrochemical performance evaluation.

Material Characterizations and Electrochemical Performance Evaluation

Crystal phases, material morphologies, microstructures, and valence states of the as-prepared samples were characterized by powder X-ray diffractometer (XRD, Philips PW1830), field emission scanning electron microscope (FE-SEM, Hitachi S4800), transmission electron microscope (TEM, FEI Tecnai G^2 20 scanning), and X-ray photoelectron spectroscopy (XPS, Model PHI5600), respectively. Thermal conversion study of precursors was conducted on thermogravimetric analysis (TGA, Mettler Toledo) and differential scanning calorimetry (DSC, Mettler Toledo) under oxygen atmosphere. In addition, specific surface area and pore size distributions of $NiCo_2O_4$ were performed on a surface area analyzer (Quantachrome Instruments) by N_2 adsorption-desorption isotherms at 77 K. The specific surface area and pore size distribution were obtained by multi-point Brunauer–Emmett–Teller (BET) and Barrett–Joyner–Halenda (BJH) method, respectively. Electrochemical lithium storage performance and rate capability were evaluated in CR2025 coin-type cell with $NiCo_2O_4$ as working electrode, lithium metal as counter electrode, microporous membrane (Celgard® 2400) as separator, and 1 M $LiPF_6$ in 50 vol.% ethylene carbonate and 50 vol.% dimethyl carbonate as electrolyte. The working electrode was composed of 80% active $NiCo_2O_4$ materials, 10% PVdF binder, and 10% SuperP conductive carbon. Cyclic voltammetry (CV) analysis was measured in the voltage range of 0.005–3 V vs. Li^+/Li and electrochemical impedance spectra (EIS) of sea urchin-like $NiCo_2O_4$ anodes were also recorded on electrochemical station (CorrTest® Instruments) in the frequency range of 100 kHz to 0.01 Hz with an amplitude of 5 mV. Galvanostatic charge-discharge test was conducted on a battery testing system (LAND CT2001A) at room temperature. The cycling performance was conducted at a current density of 100 mA g^{-1} for 100 cycles and rate capability test was performed with various current densities ranging from 100 mA g^{-1} to 3000 mA g^{-1}.

Results and Discussion

XRD pattern in Fig. 1a suggested that the as-prepared product was face-centered-cubic $NiCo_2O_4$ of high

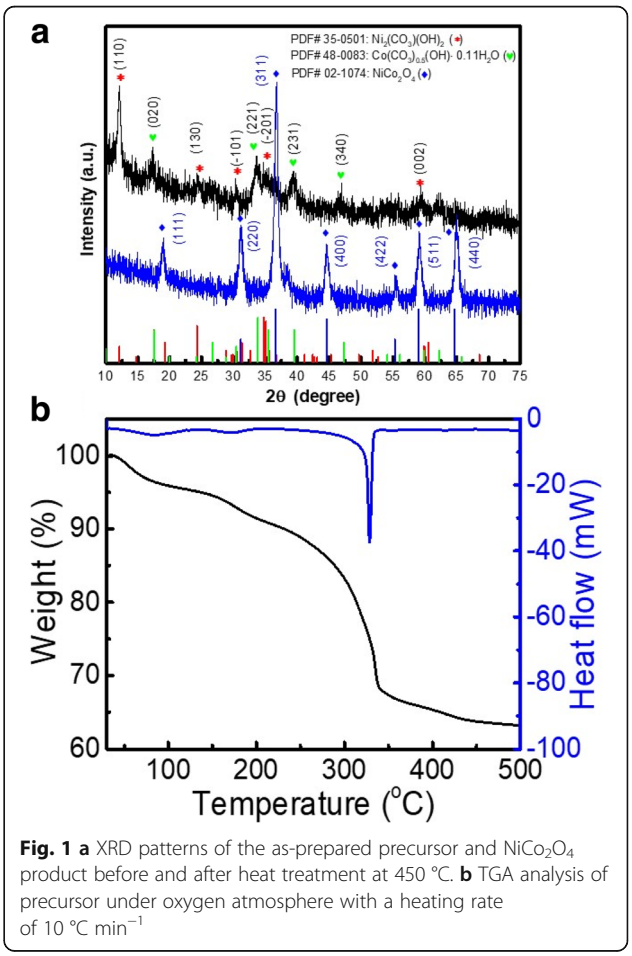

Fig. 1 **a** XRD patterns of the as-prepared precursor and $NiCo_2O_4$ product before and after heat treatment at 450 °C. **b** TGA analysis of precursor under oxygen atmosphere with a heating rate of 10 °C min^{-1}

crystallinity and purity (PDF 02-1074). The 2θ peaks located at 31.1°, 36.6°, 44.6°, 55.3°, 59.0°, 64.7° were assigned to characteristic crystal planes (2 2 0), (3 1 1), (4 0 0), (4 2 2), (5 1 1), and (4 4 0), respectively. Moreover, crystal phases in the as-prepared precursors were consisted of $Ni_2CO_3(OH)_2$ (PDF 35-0501), and $Co(CO_3)_{0.5}(OH)\cdot 0.11H_2O$ (PDF 48-0083), consistent with previous study [18]. The 2θ peaks at 12.1°, 24.3°, 30.5°, 34.8°, and 59.8° could be related to $Ni_2CO_3(OH)_2$ crystal plane (1 1 0), (1 3 0), (– 1 0 1), (– 2 0 1), and (0 0 2) respectively. The 2θ peaks at 17.5°, 33.8°, 39.5°, and 47.3° could be attributed to $Co(CO_3)_{0.5}(OH)\cdot 0.11H_2O$ crystal plane (0 2 0), (2 2 1), (2 3 1), and (3 4 0), respectively. Apparently, both Ni^{2+} and Co^{2+} were precipitated by CO_3^{2-} and OH^- ions, released from the decomposition of urea at hydrothermal conditions [16]. TGA curve in Fig. 1b displayed that calcination temperature of 450 °C was enough for thermal conversion of the mixed phases to pure $NiCo_2O_4$, since no mass loss was observed after 450 °C. Also, the conversion temperature was determined to be 350 °C, leading to a total mass loss of 37 wt %.

Morphological analysis in Fig. 2a, b implied that sea urchin-like structure of precursors was successfully obtained with PDDA-assisted hydrothermal treatment. After thermal treatment at 450 °C, sea urchin-like morphology of $NiCo_2O_4$ microspheres could still be maintained, indicating the robust nature at high temperature. The $NiCo_2O_4$ microspheres were typically ~ 2.5 μm in diameter, composed of numerous nanoneedles with an average diameter of ~ 100 nm. Note that PDDA molecules play a pivotal role in the formation of sea urchin-like structure. At the beginning, the decomposition of urea leading to generation of CO_3^{2-} and OH^- initiated the nucleation of Co^{2+} and Ni^{2+} at hydrothermal conditions. The nitrogen atoms in PDDA endowed with lone electron pairs enabled strong electrostatic interaction with negative ions. Therefore, the surface of these small nuclei was first occupied by these negative ions (CO_3^{2-} and OH^-), leading to electrostatic adsorption of positively molecules. Owing to steric hindrance, PDDA led to the crystal growth of precursors along a preferential direction. In order to minimize surface energy, self-assembly of nanostructures via a spontaneous Ostwald ripening process eventually occur, resulting in the formation of sea-urchin like structure.

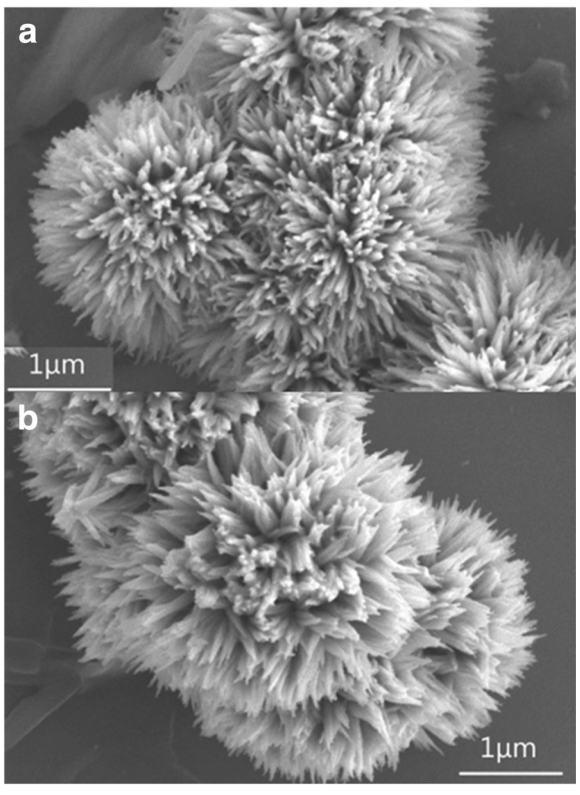

Fig. 2 **a**, **b** Typical FE-SEM images of the sea urchin-like precursor and $NiCo_2O_4$ synthesized with 5 g PDDA solution

The effects of PDDA amounts on the morphology of precursors were also investigated with FE-SEM characterization. As shown in Fig. 3, when PDDA solution of 2.5 g was added in the hydrothermal synthesis, the as-prepared precursor sample exhibited the same spherical structure of 2~5 um in diameter. Many nanoneedles, considered as the building units, were randomly organized into the large micro/nanostructured spheres. When PDDA amount was further increased to 10 g, both sea urchin-like and straw-sheaf-like structures could be obviously found in the hydrothermal precursors. The effects of PDDA on crystal orientation should be associated with the surface charge property of small nuclei, which could be tailored by the amounts of positively charged PDDA molecules. Thus, PDDA solution of 5 g, which was equivalent to a concentration of 16.7 mg L^{-1}, was the optimal conditions for synthesizing sea urchin-like structure, owing to the preferential crystal growth orientation.

The microstructures of microspheres analyzed by TEM revealed that highly porous structures in $NiCo_2O_4$ was indicated by the evident white/black contrast and high crystallinity was convinced by the clear lattice planes (Fig. 4a, b). The average size of primary particles was about 10 nm. The *d*-spacing values of ~ 0.20 nm and ~ 0.25 nm were ascribed to crystal plane (400) and (311), respectively. In addition, the pore size was about 10 nm on average. The above analysis confirmed that sea urchin-like $NiCo_2O_4$ were successfully synthesized by charge-driven self-assembly strategy with subsequent thermal treatment.

Based on N_2 adsorption-desorption isotherm, BET-specific surface area and BJH pore size distribution of $NiCo_2O_4$ sample were about 68.6 m^2 g^{-1} and 8.8 nm, respectively (Fig. 5).

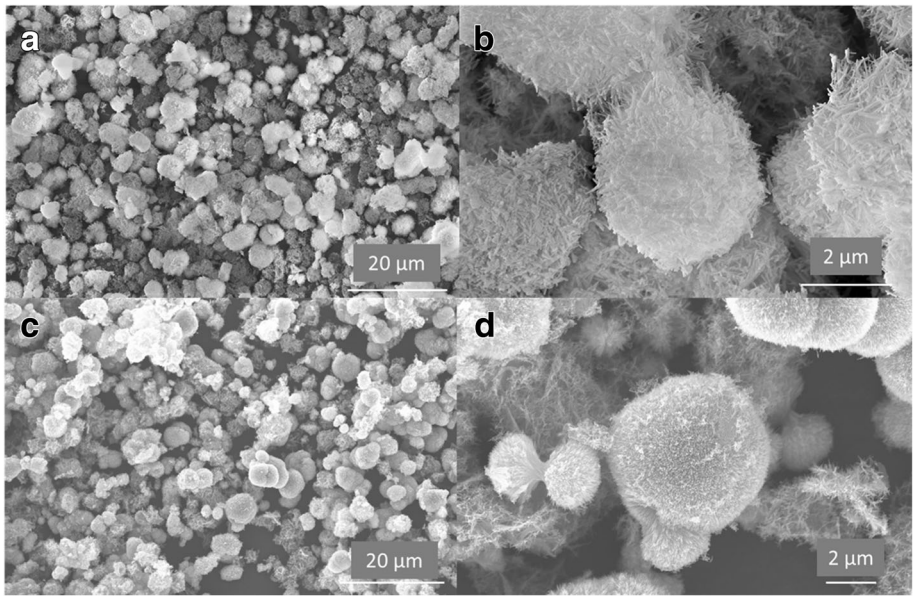

Fig. 3 Typical FE-SEM images of the as-prepared precursor synthesized with different amounts of PDDA solution **a, b** 2.5 g; **c, d** 10 g

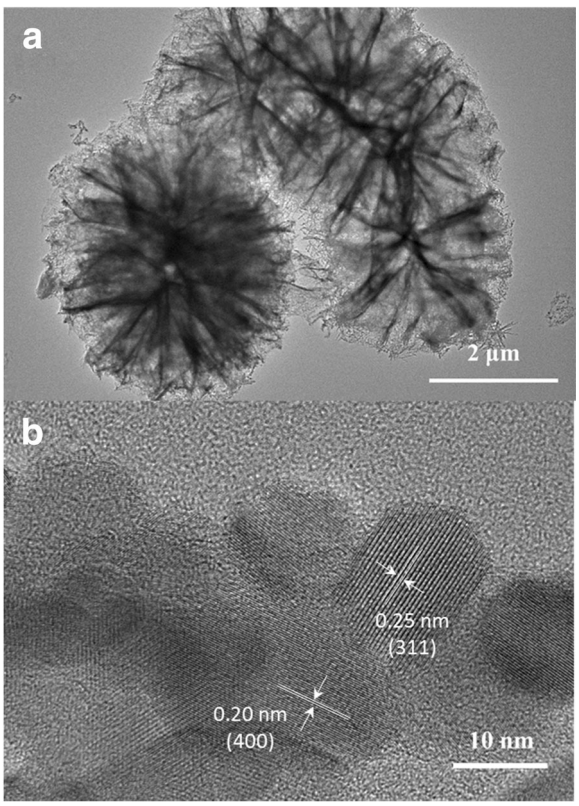

Fig. 4 a, **b** TEM images of the sea urchin-like $NiCo_2O_4$ synthesized with 5 g PDDA solution

The high surface area and uniform pore size were favorable for shortening ion diffusion length and alleviating volume expansion in electrochemical processes. The survey spectrum in Fig. 6a depicted the presence of Ni, Co, O, and C in the product. The high-resolution XPS data of Co2p in Fig. 6b indicated that co-existence of Co^{2+} and Co^{3+} species, as revealed by the fitting $Co2p_{3/2}$ peaks located at ~ 779.5 eV and ~ 781.3 eV, respectively. Similarly, high-resolution XPS data of Ni 2p in Fig. 6c implied the presence of Ni^{2+} and Ni^{3+}, as suggested by the fitting $Ni2p_{3/2}$ peaks centered at about ~ 854.6 eV and ~ 856.2 eV, respectively. The presence of satellite peaks also confirmed the presence of Co^{2+} and Ni^{2+}. Note that the peak separations for $Co2p_{1/2}$ vs $Co2p_{3/2}$ and $Ni2p_{1/2}$ vs $Ni2p_{3/2}$ were determined to be 15.2 and 17.3 eV, consistent with previous studies [16, 19]. Multiple valence states of Co (+ 2, + 3) and Ni (+ 2, + 3) in spinel $NiCo_2O_4$ were beneficial for electrochemical conversion reactions in charging-discharging processes.

The electrochemical conversion mechanism and reversibility of sea urchin-like $NiCo_2O_4$ was investigated with CV analysis. As shown in Fig. 7, in the first cycle, two distinct cathodic peaks located at about 0.8 V and 1.3 V indicated the electrochemical reduction of Co^{3+} to Co^{2+}, and then reduction of Co^{2+} and Ni^{2+} to metallic Co and Ni species, respectively [20]. For the first anodic process, electrochemical oxidation of metallic Co and Ni at about 1.4 and 2.2 V would lead to the reversible generation of Co^{2+}, Co^{3+}, and Ni^{2+} species, which eventually resulted in the formation of $NiCo_2O_4$ phase. It is also possible that solid electrolyte interphase was formed in the first activation cycle. Obviously, after the activation process in the first cycle, good reversibility of

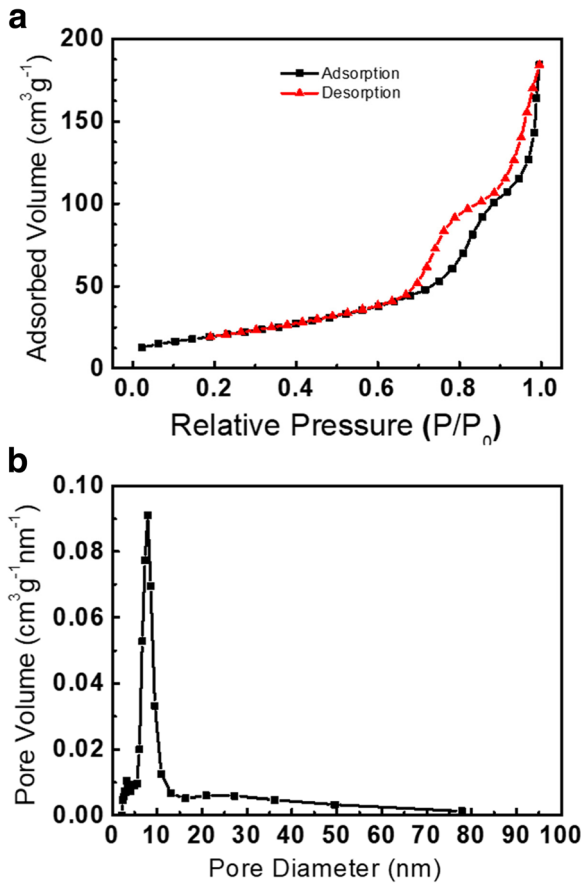

Fig. 5 a Nitrogen adsorption and desorption isotherms and **b** pore size distribution of sea urchin-like $NiCo_2O_4$ synthesized with 5 g PDDA solution

electrochemical redox reactions could be observed in the subsequent two cycles, as indicated by the overlapped CV curves. The only difference was that the major reduction peak was shifted from 0.8 to 1.0 V, consistent with previous CV study on $NiCo_2O_4$ anodes [8]. The detailed mechanism of electrochemical conversion reactions was also discussed in previous studies and could be described as below [20].

$$NiCo_2O_4 + 8\,Li^+ + 8\,e^- \leftrightarrow 2\,Co + Ni + 4\,Li_2O \quad (1)$$

$$Ni + Li_2O \leftrightarrow NiO + 2\,Li^+ + 2\,e^- \quad (2)$$

$$Co + Li_2O \leftrightarrow CoO + 2\,Li^+ + 2\,e^- \quad (3)$$

$$CoO + 1/3\,Li_2O \leftrightarrow 1/3\,Co_3O_4 + 2/3\,Li^+ + 2/3\,e^- \quad (4)$$

Electrochemical cycling performance of $NiCo_2O_4$ sample was provided in Fig. 8a and the result indicated that a reversible capacity of 663 mAh g^{-1} was achieved at a current density of 100 mA g^{-1} after 100 charge-discharge cycles. The cycling performance was also comparable with previous study on pure $NiCo_2O_4$ material. For example, electrochemical lithium storage of hierarchical $NiCo_2O_4$ nanowire array was about 413 mAh g^{-1} when evaluated at 100 mA g^{-1} over 100 cycles [5]. However, when $NiCo_2O_4$ was modified with highly conductive additives or metal oxides, better electrochemical performance could be achieved in comparison with pristine $NiCo_2O_4$. For instance, Chen et al. reported cycling stability of pure $NiCoO_2$ was significantly improved by reduced graphene oxide and a high reversible capacity of 816 mAh g^{-1} was achieved with 80.1% capacity retention [21]. Also, Sun et al. reported the cycling performance of porous $NiCoO_2$/NiO hollow dedecahedron was about 1535 mAh g^{-1} at 200 mA g^{-1} over 100 cycles, equivalent to a capacity retention of 97.2% [22]. The Coulombic efficiencies after the initial activation were almost stabilized at ~ 100%, indicative of high electrochemical reversibility. As shown in Fig. 8b, the charge-discharge curves at different cycles also showed distinctive behaviors. With repeated charge-discharge cycles, it is obvious that charge-discharge curves of the 50th cycle were also identical with the initial cycles, indicating similar electrochemical reaction pathways in the first 50 cycles. However, the

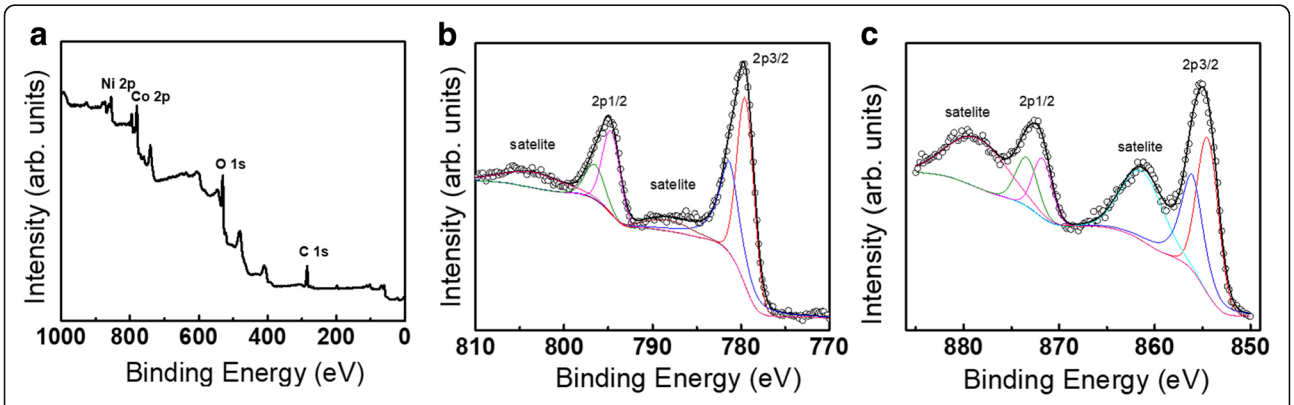

Fig. 6 a Survey spectrum of sea urchin-like $NiCo_2O_4$. **b**, **c** High-resolution XPS spectra of Co2p and Ni2p

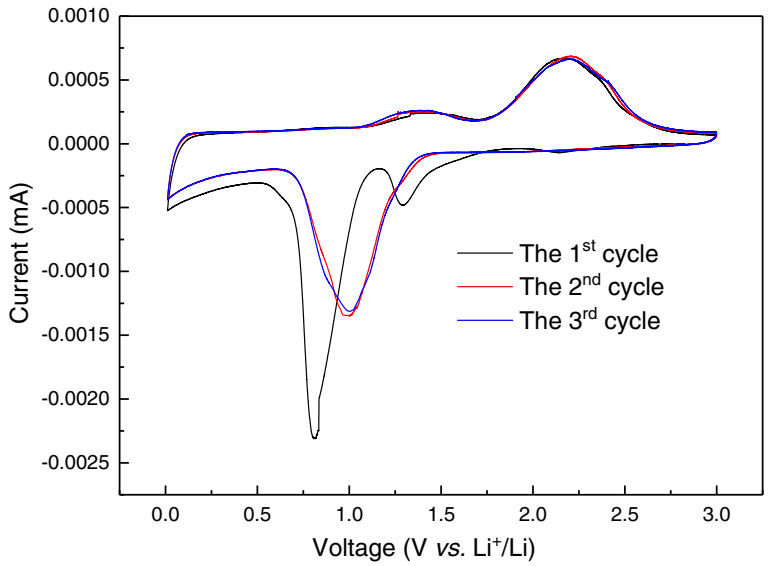

Fig. 7 Cyclic voltammetry (CV) analysis of sea urchin-like $NiCo_2O_4$ anodes in the voltage range of 0.005–3.0 V with a scanning rate of 0.01 mV s^{-1}

charge-discharge curves of the 100th cycle showed slightly different behaviors, suggesting that slow material decay might be present during the anodic conversion reactions. Moreover, rate capability in Fig. 8c showed that the average discharge capacities of $NiCo_2O_4$ measured at current densities 100, 200, 500, 1000, 2000, and 3000 mA g^{-1} were about 1085, 1048, 926, 642, 261, and 86 mAh g^{-1}, respectively. When current density was switched to 100 mA g^{-1}, high reversible capacity of about 1000 mAh g^{-1} was still maintained, indicating no obvious decay of reversible capacity in rate capability test. Note that the experimental specific capacity of 1085 mAh g^{-1} achieved at 100 mA g^{-1} was higher than theoretical value (890 mAh g^{-1}). This phenomenon was commonly observed in transition metal oxide anodes. The extra capacity might be ascribed to reversible formation of gel-like polymer films and interfacial

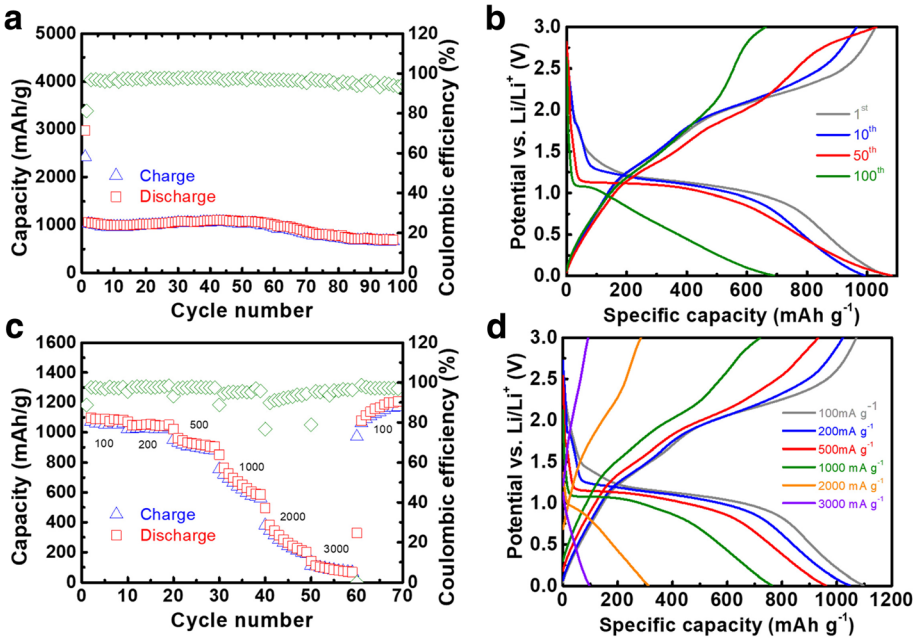

Fig. 8 a Cycling performance of $NiCo_2O_4$ tested at a current density of 100 mA g^{-1}. **b** Typical charge-discharge curves of $NiCo_2O_4$ tested at 100 mA g^{-1} for the 1st, 10th, 50th, and 100th cycle **c** rate capability performance. **d** Typical charge-discharge curves of $NiCo_2O_4$ tested at different current densities ranging from 100 to 3000 mA g^{-1}

lithium storage, etc. [23, 24]. In Fig. 8d, the typical charge-discharge curves at different current densities also suggested the specific capacity showed significant decrease with the increasing of charge-discharge current densities from 100 to 3000 mA g^{-1}. The electrochemical performance achieved in this study was better or comparable with previous studies on $NiCo_2O_4$-based materials. For instance, Chen et al. reported mesoporous $NiCo_2O_4$ nanowires delivered reversible capacities of 1215, 797, and 413 mAh g^{-1} at current densities of 200, 500, and 1000 mA g^{-1}, respectively [5]. The achieved rate capability of $NiCo_2O_4$ in this study was also comparable with previous work on other transition metal oxides. For example, Lyu et al. reported that reversible capacities of hollow CuO at evaluated current densities of 100, 200, 500, and 1000 mA g^{-1} were 629, 567, 488, and 421 mAh g^{-1}, respectively [25]. It should be mentioned that the rate performance of sea urchin-like $NiCo_2O_4$ was not stable, particularly at high current densities. This phenomenon was probably due to semiconducting nature of pristine $NiCoO_2$ and destruction of building units (nanoneedles) by high current density. Similarly, the C-rate performances of spherical $NiCo_2O_4$ and $NiCo_2O_4$ nanoribbons were also unstable in previous studies, when charge-discharge current density was changed to ≥ 1000 mA g^{-1} [20, 26].

Note that fluctuation of coulombic efficiency was also observed in the C-rate measurement, particularly at the changing points of current densities. For instance, when the current density was switched from 1000 to 2000 mA g^{-1}, coulombic efficiency of the 40th cycle was suddenly declined from 100 to about 80%. In the following 9 cycles, coulombic efficiency was immediately stabilized at about 100%. The sudden drop of coulombic efficiency might be related to the partial loss of electrical connectivity between $NiCo_2O_4$ materials and conductive network by volume variation in the charging process, due to the applied high current density. Similar phenomena were also reported in previous C-rate studies on anode materials for rechargeable batteries [27, 28].

To understand the nature of $NiCo_2O_4$ anodes, EIS analysis was conducted in the frequency range of 100 kHz to 0.01 Hz with an amplitude of 5 mV. EIS was widely employed as a useful tool to reveal electrochemical behaviors and charge transfer process [29, 30]. For $NiCo_2O_4$ anodes tested with different cycles, EIS spectra in Fig. 9 revealed small semicircles and straight lines in the high and low frequency regions, respectively. The small semicircles should be related to charge transfer resistance between electrode and electrolyte. The straight lines indicated the Warburg impedance, which should be associated with solid state diffusion of Li^+ in $NiCo_2O_4$ electrodes [8]. The charge transfer resistances of fresh $NiCo_2O_4$ electrode before and after 5 cycles were almost identical, indicating no obvious change in electrode/electrolyte interface. However, after 10 cycles, charge transfer resistance became dominant in electrochemical processes, as indicated by a larger diameter of semicircle. In addition, the nearly parallel lines suggested the same solid-state Li^+ diffusion behaviors before and after cycling tests. Therefore, charge transfer resistance of $NiCo_2O_4$ anodes could play a relatively important role in the electrochemical performance.

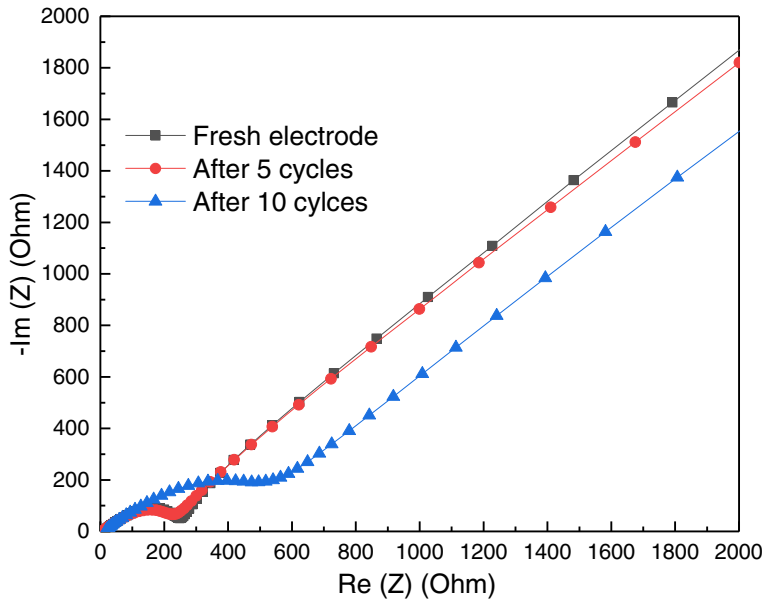

Fig. 9 EIS spectra of sea urchin-like $NiCo_2O_4$ anodes after different cycling tests in a coin cell

In this study, the improved performance of $NiCo_2O_4$ should be attributed to the micro/nanostructures of sea urchin-like morphology, compared to previous work on nanostructures (e.g., mesoporous nanowires). Basically, the lithium storage performance was associated with efficient transport of lithium ions and electrons in electrochemical charge-discharge cycles. The numerous nanoneedle, viewed as the building unit of sea urchin-like structure, could greatly improve solid-state Li^+ diffusion behaviors, due to the shortened nanoscale length. In addition, the uniform microspheres, regarded as the secondary particles of sea urchin-like structure, could significantly enhance electron transport behaviors, owing to long-range electron transport network. The combined benefits of micro/nanostructures in sea urchin-like structure could result in better electrochemical performance than nanostructures. Overall, the superior electrochemical performance of $NiCo_2O_4$ was ascribed to the unique physical properties of sea urchin-like structure, which were tailored by PDDA-assisted charge-driven self-assembly strategy. This proposed strategy has potential in facile synthesis of energy storage materials for next generation LIBs.

Conclusions

In conclusion, sea urchin-like $NiCo_2O_4$ were successfully synthesized by charge-driven self-assembly strategy with positively charged PDDA, followed by thermal treatment. The charged molecules play a pivotal role in the formation of sea urchin-like structure, due to electrostatic adsorption and steric hindrance. Also, sea urchin-like $NiCo_2O_4$ demonstrated great potentials in electrochemical lithium storage. The superior performance was ascribed to the unique sea urchin-like structure of $NiCo_2O_4$ for enhanced electron and ion transport. Overall, charge-driven self-assembly strategy is an appealing route to synthesize energy storage materials for high-performance lithium-ion batteries.

Abbreviations

BET: Brunauer–Emmett–Teller; BJH: Barrett–Joyner–Halenda; CV: Cyclic voltammetry; DSC: Differential scanning calorimetry; EIS: Electrochemical impedance spectra; FE-SEM: Field emission scanning electron microscope; LIBs: Lithium-ion batteries; PDDA: Poly(diallydimethylammonium chloride); TGA: Thermogravimetric analysis; TMOs: Transition metal oxides; XPS: X-ray photoelectron spectroscopy; XRD: X-ray diffractometer

Acknowledgements

This research was financially supported by Hong Kong Competitive Research Funding for Faculty Development Scheme (No.: UGC/FDS25/E07/16). Also, support from Hong Kong Environment and Conservation Fund (No.: 22/2016) and National Natural Science Foundation of China (No.: 51708358) were gratefully acknowledged.

Availability of Data and Materials

All data generated or analyzed during this study are included in this published article.

Authors' Contributions

XYL conceived the idea and designed the experiments. BW, CWT, KHL, and XYL performed material synthesis, electrochemical performance evaluation, and analyzed the data. YYT and YPM supported in the material characterizations. BW, KHL, CWT, and XYL contributed in the manuscript preparation. XYL supervised this work and finalized the manuscript. All authors discussed the results and approved the final manuscript.

Competing Interests

The authors declare that they have no competing interests.

Publisher's Note

Author details

[1]Faculty of Science and Technology, Technological and Higher Education Institute of Hong Kong, Hong Kong, People's Republic of China. [2]Hong Kong Applied Science and Technology Research Institute, Hong Kong, People's Republic of China. [3]School of Environmental Science and Engineering, Southern University of Science and Technology, Shenzhen, People's Republic of China. [4]Department of Chemistry and Environmental Engineering, Shenzhen University, Shenzhen, People's Republic of China.

Received: 12 April 2018 Accepted: 23 November 2018
Published online: 07 January 2019

References

1. Li Y, Hasin P, Wu Y (2010) $Ni_xCo_{3-x}O_4$ nanowire arrays for electrocatalytic oxygen evolution. Adv Mater 22:1926–1929
2. Shen L, Yu L, Yu XY, Zhang X, Lou XWD (2015) Self-templated formation of uniform $NiCo_2O_4$ hollow spheres with complex interior structures for lithium-ion batteries and supercapacitors. Angew Chem Int Ed 54:1868–1872
3. Leng J, Wang Z, Li X, Guo H, Li H, Shih K, Yan G, Wang J (2017) Accurate construction of a hierarchical nickel-cobalt oxide multishell yolk-shell structure with large and ultrafast lithium storage capability. J Mater Chem A 5:14996–15001
4. Yuan C, Li J, Hou L, Zhang X, Shen L, Lou XW (2012) Ultrathin mesoporous $NiCo_2O_4$ nanosheets supported on Ni foam as advanced electrodes for supercapacitors. Adv Funct Mater 22:4592–4597
5. Chen G, Yang J, Tang J, Zhou X (2015) Hierarchical $NiCo_2O_4$ nanowire arrays on Ni foam as an anode for lithium-ion batteries. RSC Adv 5:23067–23072
6. Chen J, Ru Q, Mo Y, Hu S, Hou X (2016) Design and synthesis of hollow $NiCo_2O_4$ nanoboxes as anodes for lithium-ion and sodium-ion batteries. Phys Chem Chem Phys 18:18949–18957
7. Hu J, Li M, Lv F, Yang M, Tao P, Tang Y, Liu H, Lu Z (2015) Heterogeneous $NiCo_2O_4$@polypyrrole core/sheath nanowire arrays on Ni foam for high performance supercapacitors. J Power Sources 294:120–127
8. Li J, Xiong S, Liu Y, Ju Z, Qian Y (2013) High electrochemical performance of monodisperse $NiCo_2O_4$ mesoporous microspheres as an anode material for Li-ion batteries. ACS Appl Mater Interfaces 5:981–988
9. Jadhav HS, Kalubarme RS, Park C-N, Kim J, Park C-J (2014) Facile and cost effective synthesis of mesoporous spinel $NiCo_2O_4$ as an anode for high lithium storage capacity. Nanoscale 6:10071–10076
10. Shen L, Che Q, Li H, Zhang X (2014) Mesoporous $NiCo_2O_4$ nanowire arrays grown on carbon textiles as binder-free flexible electrodes for energy storage. Adv Funct Mater 24:2630–2637
11. Mondal AK, Su D, Chen S, Kretschmer K, Xie X, Ahn HJ, Wang G (2015) A microwave synthesis of mesoporous $NiCo_2O_4$ nanosheets as electrode materials for lithium-ion batteries and supercapacitors. Chemphyschem 16:169–175
12. Mondal AK, Su D, Chen S, Xie X, Wang G (2014) Highly porous $NiCo_2O_4$ nanoflakes and nanobelts as anode materials for lithium-ion batteries with excellent rate capability. ACS Appl Mater Interfaces 6:14827–14835
13. Song Y, Zhao M, Li H, Wang X, Cheng Y, Ding L, Fan S, Chen S (2018) Facile preparation of urchin-like $NiCo_2O_4$ microspheres as oxidase mimetic for colormetric assay of hydroquinone. Sens Actuator B-Chem 255:1927–1936
14. Xu J, He L, Xu W, Tang H, Liu H, Han T, Zhang C, Zhang Y (2014) Facile synthesis of porous $NiCo_2O_4$ microflowers as high-performance anode materials for advanced lithium-ion batteries. Electrochim Acta 145:185–192

15. Wang B, Tang Y, Lu X-Y, Fung SL, Wong KY, Au WK, Wu P (2016) Rectangular Co_3O_4 with micro–/nanoarchitectures: charge-driven PDDA-assisted synthesis and excellent lithium storage performance. Phys Chem Chem Phys 18:4911–4923
16. Wang B, Lu X-Y, Tsang C-W, Wang Y, Au WK, Guo H, Tang Y (2018) Charge-driven self-assembly synthesis of straw-sheaf-like Co_3O_4 with superior cyclability and rate capability for lithium-ion batteries. Chem Eng J 338:278–286
17. Zhang Y, Ma M, Yang J, Su H, Huang W, Dong X (2014) Selective synthesis of hierarchical mesoporous spinel $NiCo_2O_4$ for high-performance supercapacitors. Nanoscale 6:4303–4308
18. Lei Y, Wang Y, Yang W, Yuan H, Xiao D (2015) Self-assembled hollow urchin-like $NiCo_2O_4$ microspheres for aqueous asymmetric supercapacitors. RSC Adv 5:7575–7583
19. Iacomi F, Calin G, Scarlat C, Irimia M, Doroftei C, Dobromir M, Rusu GG, Iftimie N, Sandu AV (2011) Functional properties of nickel cobalt oxide thin films. Thin Solid Films 520:651–655
20. Li B, Feng J, Qian Y, Xiong S (2015) Mesoporous quasi-single-crystalline $NiCo_2O_4$ superlattice nanoribbons with optimizable lithium storage properties. J Mater Chem A 3:10336–10344
21. Chen Y, Zhuo M, Deng J, Xu Z, Li Q, Wang T (2014) Reduced graphene oxide networks as an effective buffer matrix to improve the electrode performance of porous $NiCo_2O_4$ nanoplates for lithium-ion batteries. J Mater Chem A 2:4449–4456
22. Sun C, Yang J, Rui X, Zhang W, Yan Q, Chen P, Huo F, Huang W, Dong X (2015) MOF-directed templating synthesis of a porous multicomponent dodecahedron with hollow interiors for enhanced lithium-ion battery anodes. J Mater Chem A 3:8483–8488
23. Lee KJ, Kim T-H, Kim TK, Lee JH, Song H-K, Moon HR (2014) Preparation of Co_3O_4 electrode materials with different microstructures via pseudomorphic conversion of co-based metal–organic frameworks. J Mater Chem A 2: 14393–14400
24. Bian S-W, Zhu L (2013) Template-free synthesis of mesoporous Co_3O_4 with controlled morphologies for lithium ion batteries. RSC Adv 3:4212–4215
25. Lyu F, Yu S, Li M, Wang Z, Nan B, Wu S, Cao L, Sun Z, Yang M, Wang W, Shang C, Lu Z (2017) Supramolecular hydrogel directed self-assembly of C- and N-doped hollow CuO as high-performance anode materials for Li-ion batteries. Chem Comm 53:2138–2141
26. Li T, Li X, Wang Z, Guo H, Li Y (2015) A novel $NiCo_2O_4$ anode morphology for lithium-ion batteries. J Mater Chem A 3:11970–11975
27. Serino AC, Ko JS, Yeung MT, Schwartz JJ, Kang CB, Tolbert SH, Kaner RB, Dunn BS, Weiss PS (2017) Lithium-ion insertion properties of solution-exfoliated Germanane. ACS Nano 11:7995–8001
28. Choudhury S, Zeiger M, Massuti-Ballester P, Fleischmann S, Formanek P, Borchardt L, Presser V (2017) Carbon onion–sulfur hybrid cathodes for lithium–sulfur batteries. Sustain Energy Fuels 1:84–94
29. Shi Z, Lu H, Liu Q, Cao F, Guo J, Deng K, Li L (2014) Efficient p-type dye-sensitized solar cells with all-nano-electrodes: $NiCo_2S_4$ mesoporous nanosheet counter electrodes directly converted from $NiCo_2O_4$ photocathodes. Nanoscale Res Lett 9:608
30. Wu S, Wang W, Li M, Cao L, Lyu F, Yang M, Wang Z, Shi Y, Nan B, Yu S, Sun Z, Liu Y, Lu Z (2016) Highly durable organic electrode for sodium-ion batteries via a stabilized α-C radical intermediate. Nat Commun 7:13318